


## II Unileg Thermoelectric Structure for Cycling Robustness at High Temperature and Low Manufacturing Cost

GUSTAVO GARCÍA <sup>1,4</sup> PABLO MARTÍNEZ-FILGUEIRA,<sup>1</sup>  
MARTA CORDON,<sup>1</sup> IDOIA URRUTIBEASCOA,<sup>2</sup> ANDRÉS SOTELO,<sup>3</sup>  
JUAN CARLOS DIEZ,<sup>3</sup> MIGUEL ANGEL TORRES,<sup>3</sup>  
and MARÍA A. MADRE<sup>3</sup>

1.—CS Centro Stirling S. Coop., Avda. Álava 3, 20550 Aretxabaleta, Spain. 2.—Materials and Forming Department, Faculty of Engineering, Mondragon University, Mondragon, Spain. 3.—ICMA (CSIC-Universidad de Zaragoza), Maria de Luna 3, 50018 Saragossa, Spain. 4.—e-mail: ggarcia@centrostirling.com

Unileg-type thermoelectric generators have proven to be a good choice for high-temperature applications, because their composition from a single thermoelectric material avoids different thermal expansion coefficients, giving the structure good mechanical strength and increased lifespan during thermal cycling. These structures are usually composed of a thermoelectric pellet with metallic electrical conductors joining the hot and cold ends of consecutive pellets. The novel unileg structure described herein is designed to deal with one of the main issues with traditional devices, viz. the physical and chemical stability of the solder between the pellet and the conductor at the hot side. The material for which this structure is proposed is a *p*-type  $\text{Ca}_3\text{Co}_4\text{O}_9$  semiconductor oxide, due to its chemical stability at high temperature and good machinability. This final requirement is related to the main innovation of the structure, viz. a partial cut that divides the pellet longitudinally, leaving two legs joined by an uncut section, forming a section similar to the letter II. The metallic conductor stripe usually employed in unileg thermoelectric generator manufacturing is replaced by a coating of conductive material, in this case silver, on one of the legs resulting from the cut. Due to these operations, one of the legs is practically short-circuited and acts as an electrical conductor for the unileg structure, eliminating the need for soldering at the hot end of the pellet.

**Key words:** Unileg, thermoelectric generator, thermal stress, power generation, thermal simulation, energy efficiency

### INTRODUCTION

The increasing industrialization of network-connected devices and the real-time monitoring of industrial processes, which require a supply of electrical energy, have led to increasing popularity in waste energy harvesting systems. Such harvesters include thermoelectric generators, which are solid-state devices that can convert a thermal flow passing through them into electrical energy

due to the physical phenomenon called the thermoelectric effect. These energy harvesting devices have also been used as main electrical energy sources, due to one of their main advantages over other engines, i.e., their independence from the fuel used to raise the temperature of the hot side, as seen in radioisotope thermoelectric generators used in space probes<sup>1</sup> or natural-gas-fueled thermoelectric generators for unattended installations with high reliability requirements.<sup>2</sup>

Thermoelectric generators are usually composed of pellet-shaped semiconductor thermoelectric material and strips of conductive material of metallic nature that connect the pellets, on substrates of

(Received August 20, 2018; accepted January 8, 2019; published online January 23, 2019)

ceramic or metallic material, where the hot and cold sources of the system are located. These pellets are connected thermally in parallel and electrically in series. The most common structure is that formed by alternating *n*- and *p*-type semiconductors, such as the one shown in Fig. 1a.

Another structure is the so-called unileg. In this design, only one semiconductor material is used. This is usually done due to the lack of a semiconductor material of the other type having similar properties, or as a way to avoid stresses deriving from different coefficients of thermal expansion, which is a common effect in high-temperature modules, where thermal gradients can lead to device failure on thermal cycling. As seen in Fig. 1b, a Z-folded metallic stripe usually joins the hot and cold ends of the pellets of the same material in the unileg case.<sup>3</sup> This part is significantly more complicated from a geometrical point of view than the equivalent in a conventional module, representing a challenge when manufacturing the module repeatedly, precisely, and as close as possible to the ideal design.<sup>4</sup> Modules built without using any special fabrication process can reach manufacturing factor ( $MF = R_{ideal}/R_{int}$ ) values, as defined by Lemonnier et al.,<sup>5</sup> of around 60%.<sup>6</sup> Simplification of unileg modules is the subject of numerous patents,<sup>7,8</sup> where exotic forms of connectors and mechanisms to ease the assembly process can be found.

The conversion efficiency of such devices is represented by the figure of merit  $ZT$ , which relates thermal parameters such as the thermal conductivity and temperature and electrical parameters such as the resistivity and Seebeck coefficient.

$$ZT = \frac{\alpha^2 \sigma}{k} T.$$

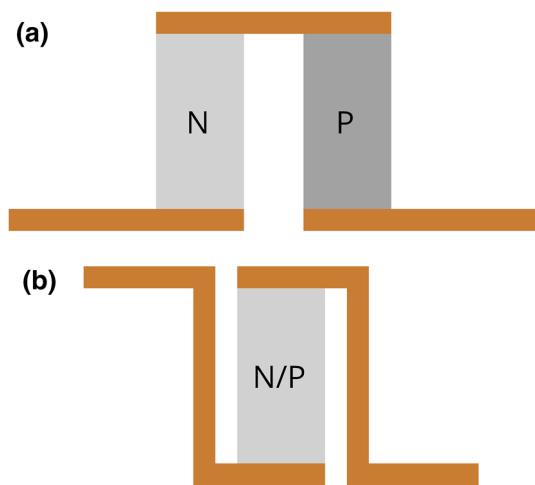


Fig. 1. The most common thermoelectric structures employed for module building using (a) *n*- and *p*-type semiconductors or (b) only one type.

For years, research efforts have focused on achieving  $ZT$  values that would allow use in practical power generation applications, on the order of  $ZT \approx 1.5$ , by improving the power factor  $\alpha^2 \sigma$ , by improving the Seebeck coefficient, increasing the electrical conductivity, or reducing the thermal conductivity of the materials. However, few studies or inventions have tried to improve the overall efficiency of thermoelectric modules by means of geometric modifications to the classic setup.<sup>9</sup>

The viability of thermoelectric modules as a source of electrical energy depends on a balance between their efficiency, cost, and ecological impact. In the work described herein, we developed a basic module structure that aims to reduce the cost of the whole assembly using a *p*-type oxide semiconductor material ( $Ca_3Co_4O_9$ ), which also has the advantage of complying with Restriction of Hazardous Substances (RoHS) regulations, making it a safe material. Because of the use of a single thermoelectric material, the structure can be considered to be of unileg type. This material was chosen for its good machinability and physical and chemical stability at high temperatures.<sup>10</sup>

The machinability requirement is related to the main innovation of the structure, viz. a cut that divides the thermoelectric pellet into two segments joined by an upper section that is not affected by the mentioned cut, forming a section that resembles the Greek letter Π. The metallic stripe typically used in unileg assemblies is replaced by a coating of metallic material, preferably silver due to its high melting point and electrical conductivity, on one of the segments resulting from the cut. In this way, it is expected to achieve an effect similar to an electrical short circuit, due to the high electrical conductivity of the metallic coating, similar to what occurs with the metallic stripe that is commonly used. Figure 2 compares a conventional unileg device with the device having the proposed new structure.

This development involves the same number of welds, viz. two, for each basic thermoelectric unit. However, the proposed configuration offers an advantage over the conventional unileg in that both

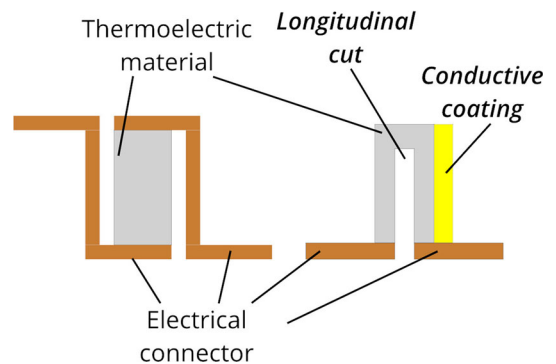


Fig. 2. Comparison of the current most commonly used unileg solution (left) with the proposed novel structure (right).

welds to be made can be placed on the side designated as the cold focus of the system, using solder paste with a lower melting temperature, which enables use of lower-temperature manufacturing processes that avoid the diffusion of materials that occurs in the hot focus at high temperatures.<sup>11,12</sup> Formation of intermetallic compounds between the thermoelectric material and solder is unfavorable due to their weak mechanical strength and high contact resistance.<sup>13</sup> The lifespan of the thermoelectric module is also improved because, being composed of only a single thermoelectric material, there are no expansion stresses, which is of special importance for devices subjected to high temperatures and large thermal gradients, which could fracture the module.

The aim of this work is to compare the theoretical thermoelectric behavior expected from the new structure with a single pellet, to reveal how the special features of this invention will affect the performance of the material.

### TEG MODELING

To understand the behavior of this particular structure theoretically, a tailor-made finite difference solver was developed using the core MATLAB package. The equations of the physics involved in this problem, Eqs. 1 and 2, are solved iteratively at each time step. The transient term of the electrical field equation is not taken into account.

$$\rho C_p \frac{\partial T}{\partial t} - \nabla(k \nabla T) = \rho_{el} J^2 + T J \nabla \alpha, \quad (1)$$

$$\nabla V = -\alpha \nabla T - \rho_{el} J. \quad (2)$$

The first term on the right-hand side of Eq. 1 is the volumetric contribution of the Joule effect to the heat generation, while the second one is related to the Peltier and Thompson effects. The electric field in Eq. 2 is governed by the voltage difference caused by the Seebeck effect and the voltage drop caused by the resistivity of the material. For the numerical analysis, it is useful to handle these separately.

In the calculations performed in this work, *p*-type Bi<sub>2</sub>Te<sub>3</sub> semiconductor was considered as the thermoelectric material, as the temperature-dependent

properties of Ca<sub>3</sub>Co<sub>4</sub>O<sub>9</sub> obtained using an improved manufacturing process<sup>14</sup> were not yet available when starting this work. The thermal and electrical conductivities and Seebeck coefficient were set to be temperature dependent for Bi<sub>2</sub>Te<sub>3</sub> according to the polynomials whose coefficients are presented in Table I. The conductive material is a 35- $\mu$ m-thick silver layer with all thermal and electrical properties constant. It is attached to a 2.5-mm-side square-base prism with a 10-mm-high thermoelectric element. The cut is centered and 0.5 mm wide, with depth of 8.5 mm. In the single-pellet calculation, a pellet of the same size was considered, in this case without the coating or cut. It has to be taken into account that no metallic stripes are considered in this computation. A simple calculation is used to estimate its performance,<sup>15</sup> as this simple geometry does not require finite difference analysis.

Figure 3 shows the computational domain, with a variable-spacing mesh to properly capture the effects and gradients near the silver layer. The solid silver layer is modeled without thermal or electrical contact resistance. Figure 4a and b show the thermal and electrical boundary conditions used in the analysis, with fixed temperature of 85°C at the hot side and uniform heat flux at the cold side, and the electrical reference set at the non-short-circuited leg. The thermal power dissipated at the cold end is 50 mW.

A mesh independence study was conducted to ensure that the results were not dependent on the grid quality, using the Richardson extrapolation method<sup>16</sup> by which a higher-order estimation of the thermal and electrical fields can be estimated from a series of low-order discrete values. The value estimated by Richardson extrapolation is that which would be obtained if the grid size tended to zero. Three different grid levels were used for this calculation, with a mesh refinement ratio of four between consecutive levels. The finest grid contained nearly 17,000 cells. Strong dependence on grid size was found, especially at the open-circuit voltage, which is a consequence of the Seebeck effect and substantially influences the other results. As discussed below, the possible cause of this phenomenon can be clearly appreciated in Fig. 5. All variables converge asymptotically and monotonically, which is why this extrapolation method can be used.

**Table I. Thermoelectric properties of Bi<sub>2</sub>Te<sub>3</sub> employed in the numerical analysis**

Property	Polynomial Coefficients $P = a_4 T^4 + a_3 T^3 + a_2 T^2 + a_1 T^1 + a_0$				
	$a_4$	$a_3$	$a_2$	$a_1$	$a_0$
Thermal conductivity, $\kappa$ (W m <sup>-1</sup> K <sup>-1</sup> )	$-2.002 \times 10^{-11}$	$-5.033 \times 10^{-8}$	$4.010 \times 10^{-5}$	$-1.638 \times 10^{-3}$	$1.485 \times 10^0$
Electrical conductivity, $\sigma$ ( $\Omega^{-1}$ m <sup>-1</sup> )	$7.040 \times 10^{-15}$	$-4.566 \times 10^{-12}$	$8.468 \times 10^{-10}$	$1.709 \times 10^{-8}$	$7.744 \times 10^{-6}$
Seebeck coefficient, $S$ (V K <sup>-1</sup> )	$-1.318 \times 10^{-15}$	$8.444 \times 10^{-13}$	$-1.742 \times 10^{-9}$	$1.262 \times 10^{-7}$	$2.161 \times 10^{-4}$

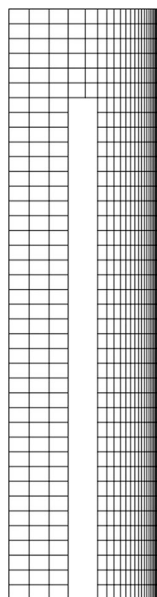


Fig. 3. Computational mesh of the new thermoelectric structure; note the cell clustering near the conductive coating.

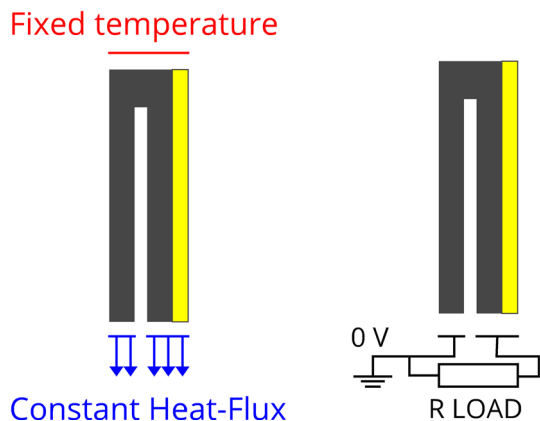


Fig. 4. Thermal and electrical boundary conditions applied in the simulation. The yellow rectangle attached to the II indicates the conductive coating (not to scale).

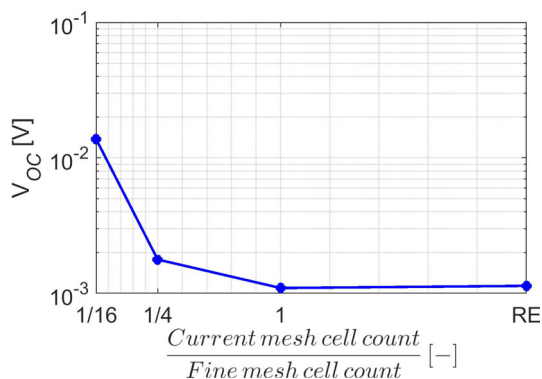


Fig. 5. Open-circuit voltage for three grid levels and its extrapolation.

## RESULTS

Each steady-state calculation was completed in less than 5 s. This calculation efficiency allowed performance of computations with a set of resistor values ranging from 0  $\Omega$  to 1.6  $\Omega$  acting as a linear load for the novel thermoelectric structure.

Figure 6 shows the output of one of these computations graphically. The thermal field seems to have been slightly influenced by the higher thermal conductivity of the conductive coating, as it reaches higher temperatures at the right leg, around 8°C. In the voltage field due to the current flow, it can be clearly seen that the voltage drop on the right side is smaller than that on the other side. This confirmed that the new structure works almost as a short circuit, as foreseen in the concept stage. Regarding the contribution of the Seebeck effect, as a consequence of the thermal distribution, the right leg has a smaller potential difference compared with the left at its ends. This creates a net potential between the terminals of the structure. Note that the voltage gradient due to the Seebeck effect is also smaller in the short-circuited leg. The resulting voltage field produces a potential difference at the base of the thermoelectric element, which corresponds to the voltage applied to the load resistor. This value is slightly higher than 1 mV.

The results for the novel thermoelectric structure are compared quantitatively with those for a single pellet in the figures presented below. As can be seen, the resulting profiles follow the same trend in both cases. However, the efficiency of the proposed structure seems to be several times lower than the values for a single pellet. It has to be taken into account that the performance degradation caused by the Z-folded stripes is not considered here. However, the efficiency of a conventional unileg system can reach values as high as 2.3%,<sup>17</sup> compared with around 3.5% in these calculations, much higher than the value of 0.013% reached by the novel structure.

Another interesting feature that can be observed from these graphs is that the internal resistance of the leg is almost three times higher than for a single pellet, as the peak value of the electrical power dissipated at the resistor is offset to higher resistor values.

The voltage applied to the load is around ten times lower for the new structure, which in combination with the higher internal resistance, results in a much smaller current of 25 mA in short-circuit conditions compared with the value of 700 mA that can be achieved with a single pellet.

## DISCUSSION

### Computational Results

As expected, the power that can be developed using this structure is lower than that which can be achieved with a single pellet. The energy harvesting

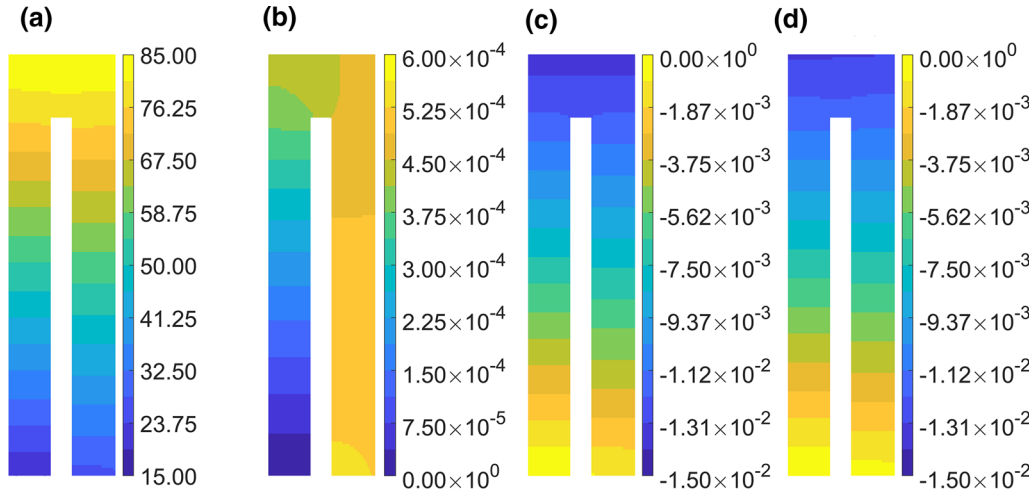


Fig. 6. Computation results showing (a) temperature field ( $^{\circ}\text{C}$ ), (b) ohmic voltage drop (V), (c) Seebeck voltage (V), and (d) resulting voltage (V) for load resistor  $R_{\text{LOAD}} = 50 \text{ m}\Omega$ , fixed hot-side temperature  $T_{\text{HOT}} = 85^{\circ}\text{C}$ , and dissipated thermal power  $Q_{\text{COLD}} = 50 \text{ mW}$ . Note the difference in voltage scale between (b) versus (c) and (d).

efficiency is reduced by two orders of magnitude. As in Fig. 6, the contributions of the temperature, voltage drop, and Seebeck effect are analyzed separately below.

The temperature field is strongly influenced by the geometry of the cut and the presence of the metallization. In this analysis, the cut was centered, resulting in two legs with the same cross-section. The metallization is  $35 \mu\text{m}$  thick, so it is a very low section with respect to the legs, of  $1 \text{ mm}$  each. Despite this great difference, the higher thermal conductivity of the silver results in asymmetry in the temperature field of the thermoelectric material. When reducing the section of the metallized leg, either by displacing or increasing the thickness of the cut and displacing it, the device would tend to behave like a conventional unileg structure. It should also be considered that, if the thermal contact resistance were taken into account, the thermal distribution could be affected. It is known that one of the sources of inefficiency of a conventional unileg device is the high thermal flux that passes through the metallic strip. Therefore, the thermal difference of the legs is expected to increase. The boundary conditions imposed in the calculation are also responsible for the resulting temperatures. To simplify the analysis, Neumann boundary conditions were applied on all parts of the assembly in contact with the cold side, prescribing the amount of heat that passes through the structure ( $\text{W}/\text{m}^2$ ). It is believed that employing a Cauchy boundary condition with an external temperature and a heat transfer coefficient could further vary the thermal field of the structure. This would be more similar to a real system, for example, a finned heat sink that acts as the cold side. In the same way, a change of the boundary condition applied on the hot side could cause the thermal flux to vary. In this case, the boundary condition is of fixed-temperature

Dirichlet type. It is expected that these changes would produce an increase in the temperature of the metallized side of the leg. The choice of these boundary conditions, albeit not ideal, was made because the authors considered this to be the best way to represent real-life power generation systems. The mentioned changes could have a direct effect on the distribution of the Seebeck coefficient along the structure.

The Seebeck coefficient distribution does not seem to be strongly affected by the presence of a material with an assigned Seebeck coefficient of zero. The value at the ends of the legs varies in proportion to the variation of the temperature field. The electric field of each leg is opposite, and it is their difference that creates the net potential difference. Any increase in the resulting voltage will increase the efficiency of the proposed structure. The mesh dependence analysis carried out in this work showed that the resulting electromotive force is sensitive to the mesh density in the metallized area. This parameter, together with the load resistance and internal resistance, also serves to determine the current flowing through the structure terminals. It is therefore of particular relevance to realize clustering of computational cells in the metallization and the area where it contacts the thermoelectric material.

Finally, with regard to the voltage drop due to the current flow, it can be said that, compared with the low voltage generated by the Seebeck effect, its effect on the total generated power is not so severe. However, the division of the leg into two halves causes the internal resistance to rise, as the electrical section through which the current must flow decreases. In this way, the voltage drop is greater than across a single pellet with larger section. The metallization practically fulfills the theory of causing an electrical short circuit. Thanks to this effect,

an even greater voltage drop is avoided, since the length to be traversed by the electric fluid would increase in the absence of this layer. As in the thermal section, taking into account the contact resistance of the silver layer could have performance implications, since the resistance to current flow would increase. This should therefore also be the object of future studies to determine the optimal ratio of the leg sections to maximize energy harvesting. However, it is possible that the optimization of this parameter will be a particular issue for each application.

### Thermoelectric Leg Concept

When considering the development of new materials and modules, efficiency improvements are generally given priority, but there are applications, mainly industrial, where other characteristics such as robustness and cost are given priority, with efficiency being relegated in importance as long as the TEG device generates the energy required for the application.

Although the level of energy generated by the proposed structure is clearly insufficient for any practical applications, the fact that it works according to the conceptual considerations reveals certain advantages over conventional designs. In this sense, the proposed design exhibits a series of characteristics that will allow improvements in terms of cost and robustness, as the calculations indicate that the new structure theoretically allows the development of a net potential difference between the legs of the structure.

The use of a single material prevents geometric distortions due to the effects of expansion, avoiding the high thermal stresses that occur in conventional thermoelectric modules when two different materials undergo contractions and dilatations of different magnitude during thermal cycling, which can result in failure and destruction of the module. The absence of welding on the hot side is one of the factors that influence the expected improvement in robustness, since welding results in a contact resistance that deteriorates with both continuous exposure to high temperature<sup>18</sup> and stresses due to thermal cycling and the mismatch of thermal expansion coefficients between various module components and materials,<sup>19</sup> although this requires experimental validation in future work.

The main barrier to production of economical high-temperature thermoelectric modules lies not in the material, but in the costs of the system, heat exchangers, and ceramic plates.<sup>12</sup> The cost of high-temperature generation modules is generally too high for commercial applications, although their use is possible in specific niches that are less conditioned by price restrictions. Apart from the TE materials used, most TE modules are assembled manually, requiring, in addition, specific welding materials and tools to withstand the high assembly

and operating temperatures. The potential of the target material,  $\text{Ca}_3\text{Co}_4\text{O}_9$ , to be machined using known and standardized methods in industry, viz. milling, drilling, and sawing, means that the proposed structure can adopt shapes from prismatic to circular crowns. In addition, multiple interconnected thermoelectric structures can be obtained from a single block of material, as shown in Fig. 7. This would have a double beneficial effect on the module: it would be more reproducible due to the lower variability in the characteristics of the elements, as all the structures are part of the same block of thermoelectric material; in addition, use of a large number of welds and interconnections in the module, which are a source of manufacturing errors and inefficiency during operation, could be avoided.

If such structures are individually manufactured and welded to form a module, only half the number of welds is needed compared with a conventional module, and less than for a conventional unileg module. The advantage with respect to the latter would be that all the joints could be made on the cold side of the module, so that thermal pastes with lower cost and lower melting temperature could be employed, potentially enabling the use of only commercial soldering materials for the cold side, with soldering temperatures above  $250^\circ\text{C}$ , as well as conventional reflow ovens that are widely used in the electronics industry. Likewise, the required tooling will work in the same temperature range, making it possible to take advantage of conventional, mature, and proven electronic assembly processes for automated manufacture of high-temperature modules. This manufacturing approach would make it possible to address niche applications with larger market volume compared with current solutions.

Obviously, in any comparison of the performance of an actual thermoelectric device or module against the pure material or ideal behavior, real devices will always show a worse response, due to the occurrence of electrical contact resistance in all assembly processes.

Lemonnier et al.<sup>5</sup> define the manufacturing factor (MF), which represents the manufacturing quality of the device as  $\text{MF} = R_{\text{ideal}}/R_{\text{int}}$ . In a real module,

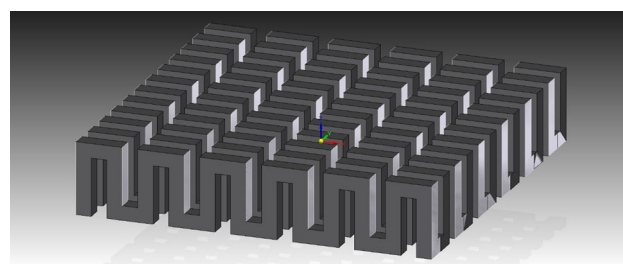


Fig. 7. Thermoelectric module made from a single machined thermoelectric material block. Lighter faces represent silver-coated legs.

contact resistances  $R_{\text{contact}}$  appear between the thermoelectric material and metal, and the internal resistance of the module  $R_{\text{int}}$  is therefore given by the ratio  $R_{\text{int}} = R_{\text{ideal}} + R_{\text{contact}}$ . The lower the value of  $R_{\text{contact}}$ , the higher the electrical power generated; the power generated will reach its maximum  $P_{\text{max}} = E_0^2/4R_{\text{int}}$ , when the load applied is  $R_L = R_{\text{int}}$ .

In a comparison made by Lemonnier et al.,<sup>5</sup> the MF of previously published oxide modules was analyzed. The results for a single  $n$ - $p$ -type uncouple module and a unileg-type module gave an MF of 0.15.

Even though we have not made a prototype to evaluate this parameter with respect to the ideal, it does provide a measure of the reduction of the internal resistance of the new proposed architecture with respect to the ideal. Figure 8 shows the maximum power generated by the new and the conventional structure. Using these load resistance values and assigning the values of  $R_{\text{ideal}} = R_{\text{conventional}} = 17.31 \text{ m}\Omega$  and  $R_{\text{int}} = R_{\text{new structure}} = 47.29 \text{ m}\Omega$  gives a value of  $\text{MF} = R_{\text{ideal}}/R_{\text{int}} = 0.36$ .

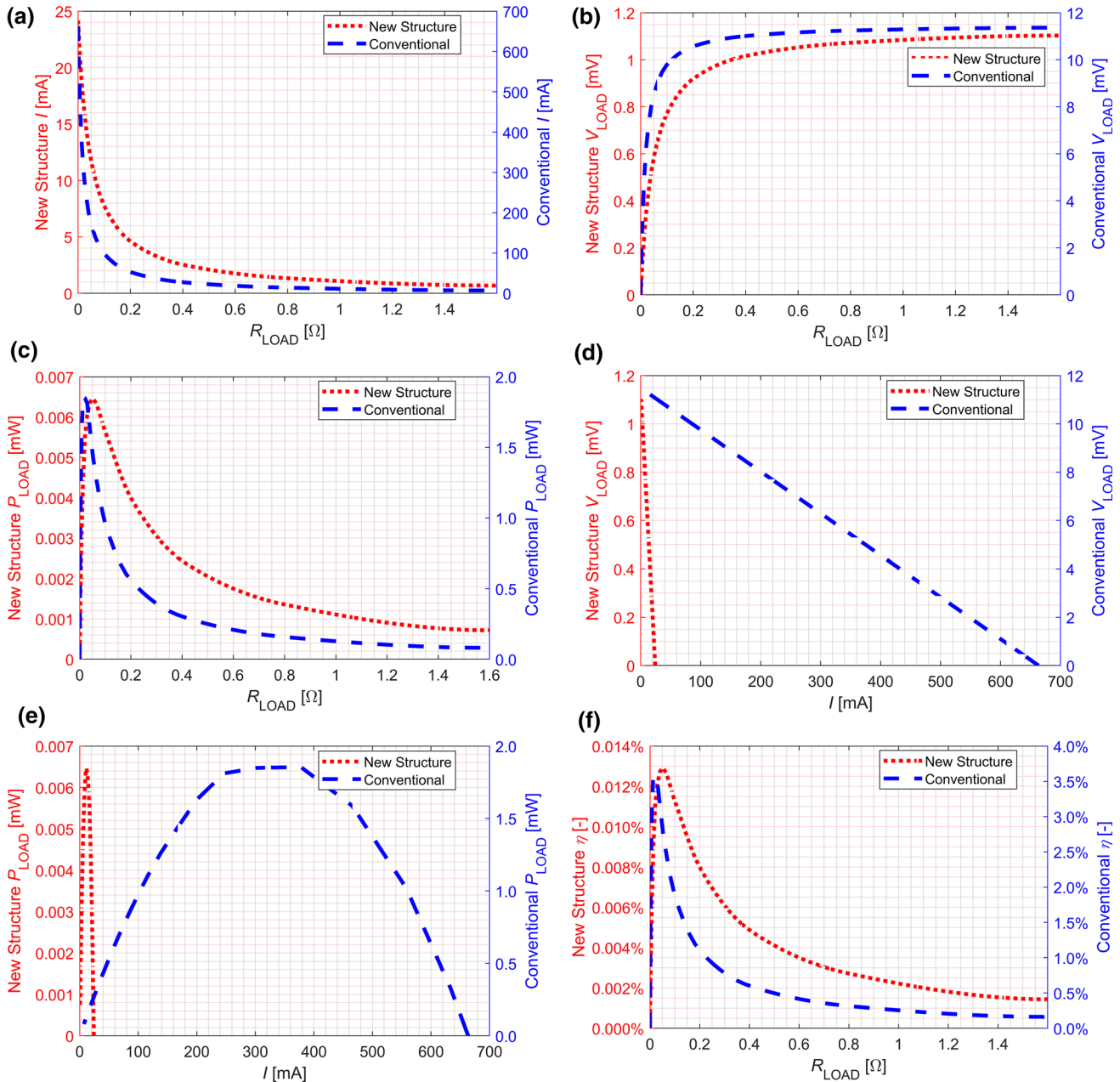


Fig. 8. Comparison of computations of new thermoelectric structure and a single pellet: (a) electric current through the load, (b) electric potential at the load and (c) electric power developed at the load with varying electric resistance load, (d) electric potential at the load and (e) electric power developed at the load with varying electric current through the circuit, and (f) thermal to electrical conversion efficiency with varying electrical resistance load.

Although this value is slightly higher than those obtained for a unileg module such as that reported by Lemonnier et al., it is far from ideal, although the cost and robustness characteristics that could be achieved to assess the validity of the new structure in certain applications must also be taken into account.

On the other hand, the module made by Lemonnier et al.<sup>5</sup> was subjected to five cycles of 10 h with a temperature difference of 360 K and a hot temperature of 760 K, so among the future steps, it is planned to evaluate the deterioration of the MF of the new structure during thermal cycling and continuous operation at high temperature.

### CONCLUSIONS

A novel thermoelectric structure was theoretically evaluated using a tailor-made finite difference thermoelectric solver, revealing the following results:

- The thermal and electrical imbalance due to the conductive coating results in a net potential difference between the legs of the structure.
- The conductive layer adhered to one of the legs of the thermoelectric element fulfills the expected function of simulating an electrical short circuit, lowering the theoretical electrical resistance compared with a structure without such a coating.
- Although this structure and material do not achieve satisfactory results for the given working conditions from the point of view of power generation, the expected conditions of high temperature and thermal cycling could cause potential applications to arise for the proposed structure.

In the future, it is planned to validate the performance of such new structures experimentally, as well as their robustness to thermal cycling, using the new  $\text{Ca}_3\text{Co}_4\text{O}_9$  material at higher temperatures, which is currently under development.

### ACKNOWLEDGMENTS

The Regional Development Agency of the Basque Country (SPRI) is gratefully acknowledged for economic support through the research project “High Temperature Oxide Module” (HITOM), KK-2017/00099, Programa ELKARTEK.

### REFERENCES

1. L. Young and B. Bairstow, Radioisotope power systems reference book for mission designers and planners. (Jet Propulsion Laboratory, National Aeronautics and Space Administration, 2015), <http://hdl.handle.net/2014/45467>. Accessed 30 Nov 2018.
2. KRYOTHERM, Ltd., Thermoelectric generators operating on gas fuel. (KRYOTHERM, Ltd., 2016), <http://kryothermt.com/thermoelectric-generators-operating-on-gas-fuel.html>. Accessed 30 Nov 2018.
3. J.W. Fergus, J. Eur. Ceram. Soc. (2012). <https://doi.org/10.1016/j.jeurceramsoc.2011.10.007>.
4. K.H. Bae, S.-M. Choi, K.-H. Kim, H.-S. Choi, W.-S. Seo, S. Lee and H.J. Hwang, J. Electron. Mater. (2015). <https://doi.org/10.1007/s11664-015-3694-8>.
5. S. Lemonnier, C. Goupil, J. Noudem, and E. Guilmeau, J. Appl. Phys. (2008). <https://doi.org/10.1063/1.2951796>.
6. E. Sudhakar Reddy, J.G. Noudem, S. Hebert and C. Goupil, J. Phys. D Appl. Phys. (2005). <https://doi.org/10.1088/0022-3727/38/19/026>.
7. H. Suda and J. Sato, Thermoelectric conversion module. U.S. Patent No. 9,537,076, 3 January 2017.
8. H. Suda, T. Nemoto, and J. Sato, Thermoelectric conversion module. U.S. Patent No. 10,003,003, 19 June 2018.
9. W. Wijesekara, L. Rosendahl, D.R. Brown, and G.J. Snyder, J. Electron. Mater. (2015). <https://doi.org/10.1007/s11664-14-3569-4>.
10. M.A. Madre, I. Urrutibeascoa, G. Garcia, M.A. Torres, A. Sotelo, and J.C. Diez, J. Electron. Mater. (2018). <https://doi.org/10.1007/s11664-018-6748-x>.
11. A.D. Gardea, R. Nishimoto, N.Y.C. Yang, A.M. Morales, S.A. Whalen, J.M. Chames, and W.M. Clift, Material compatibility and thermal aging of thermoelectric materials (Sandia National Laboratories, 2009). <https://prod.sandia.gov/techlib-noauth/access-control.cgi/2009/095968.pdf>. Accessed 30 Nov 2018.
12. S. LeBlanc, S.K. Yee, M.L. Scullin, C. Dames, and K.E. Goodson, Renew. Sustain. Energy Rev. (2014). <https://doi.org/10.1016/j.rser.2013.12.030>.
13. W.-C. Lin, Y.-S. Li, and A.T. Wu, J. Electron. Mater. (2018). <https://doi.org/10.1007/s11664-017-5906-x>.
14. M.A. Torres, G. Garcia, I. Urrutibeascoa, M.A. Madre, J.C. Diez, and A. Sotelo (2018). <https://doi.org/10.1007/s40843-018-9339-1>.
15. J.M. Gordon, Am. J. Phys. (1991). <https://doi.org/10.1119/1.16818>.
16. L.F. Richardson and J.A. Gaunt, Philos. Trans. R. Soc. A. (1927). <https://doi.org/10.1098/rsta.1927.0008>.
17. W.-H. Chen, P.-H. Wu, X.-D. Wang, and Y.-L. Lin, Energy Convers. Manag. (2016). <https://doi.org/10.1016/j.enconman.2016.09.039>.
18. F.J. Cheng, Z.L. Ma, Y. Wang, G.X. Zhang, and W.M. Long, Kovove Mater. (2014). [https://doi.org/10.4149/km\\_2014\\_3\\_157](https://doi.org/10.4149/km_2014_3_157).
19. Ferrotec Corporation USA, Thermoelectric Technical Reference. Reliability of Thermoelectric Cooling Modules. (Ferrotec Corporation USA, 2015), <https://thermal.ferrotec.com/technology/thermoelectric-reference-guide/thermalref10/>. Accessed 30 Nov 2018.